ISSN 1027-4510, Journal of Surface Investigation: X-ray, Synchrotron and Neutron Techniques, 2022, Vol. 16, No. 6, pp. 1171–1174. © Pleiades Publishing, Ltd., 2022.
Russian Text © The Author(s), 2022, published in Poverkhnost', 2022, No. 12, pp. 94–97.

Regularities of the Formation of SiO_2 Nanophases and Nanofilms on a Si Surface during O_2^+-Ion Implantation

G. Kh. Allayarova*

Karshi State University, Karshi, 180117 Uzbekistan

**e-mail: allayarova5030@mail.ru*

Received February 7, 2022; revised March 11, 2022; accepted March 11, 2022

Abstract—The implantation of O_2^+ ions in Si with an energy of $E_0 = 1$ keV followed by annealing at 850–900 K yielded nanocluster phases and SiO_2 films. Using Auger-electron spectroscopy, spectroscopy of elastically reflected slow electrons, and ultraviolet photoelectron spectroscopy, the composition, formation depths, and electronic structure of nanocluster phases and SiO_2 layers are studied. It is found that nanocluster phases and layers of SiO_2 at doses of $D \le 5 \times 10^{15}$ cm^{-2} are formed in the surface layer at a depth of 25–30 Å. With an increase in the ion dose, the SiO_2-oxide layer shifts towards the surface, and at $D \approx 6 \times 10^{16}$ cm^{-2}, a continuous SiO_2 film with a thickness of ~25–30 Å is formed. The band gap of this film is 7.9 eV.

Keywords: ion implantation, nanofilms, nanophases, ion dose, work function, band gap, photoelectrons, silicon suboxides

DOI: 10.1134/S1027451022060039

INTRODUCTION

Nanoscale structures and layers based on Si, Ge and their oxides are promising for fabricating nanoelectronic and optoelectronic devices. In particular, SiO2/Si heterostructures with various nanoinclusions serve as the basis for the development of new types of high-frequency transistors, integrated circuits, optical converters, and solar cells [1–4]. In this regard, special attention is paid to improving the technology of preparing and studying the regularities of the formation of nanoscale structures with new physical properties. Si nanoclusters in a silicon-oxide matrix are mainly produced by thermal evaporation, laser ablation, and chemical vapor deposition [5, 6]. The passivation of dangling surface bonds in the case of amorphous nanocluster phases requires subsequent annealing at $T = 623$ K in an oxygen-containing atmosphere. The ion-bombardment method is often used to manufacture nanoscale structures on the surface of semiconductors and dielectric films [7–10]. In [10], the implantation of O_2^+ ions into Si was used to fabricate nanoscale SiO_2 films with a thickness of 30–90 Å and their composition, surface morphology, emission and optical properties were studied. However, the regularities and mechanisms of the formation of SiO_2 nanofilms have not been practically studied, and the change in the density of state of valence electrons during the implantation of O_2^+ ions into Si and subsequent annealing has also not been studied. This work is devoted to studying the regularities of the formation of nanoscale SiO_2 phases and SiO_2 films during the implantation of O_2^+ into Si and the study of their composition and electronic structure.

EXPERIMENTAL

The targets were single-crystal Si(111) samples. After grinding, the samples were polished with diamond pastes until a mirror smooth surface was obtained, and then they were subjected to electropolishing in a sulfuric-methanol solution. After washing, the samples were placed in an ultrahigh vacuum device, which consists of two compartments. Annealing and ion bombardment were carried out in the first compartment. In the second compartment, the composition, electronic and optical properties were studied using a set of methods: Auger-electron spectroscopy, spectroscopy of elastically reflected slow electrons and ultraviolet photoelectron spectroscopy.

Before the implantation of O_2^+ ions, the Si samples were degassed under ultrahigh vacuum conditions ($P = 10^{-6}$ Pa), first, during long-term annealing at 1200 K for 4–5 h and then, short-term annealing at 1500 K combined with soft etching of the surface with Ar^+ ions of $E_0 = 1$ keV at an angle of 10°–15° with respect to the surface. To study the regularities of the formation of nanoscale phases and films of SiO_2, we prepared identical Si samples implanted with O_2^+ ions of $E_0 \approx 1$ keV at doses of $D = 0$, 5×10^{13}, 5×10^{14}, and

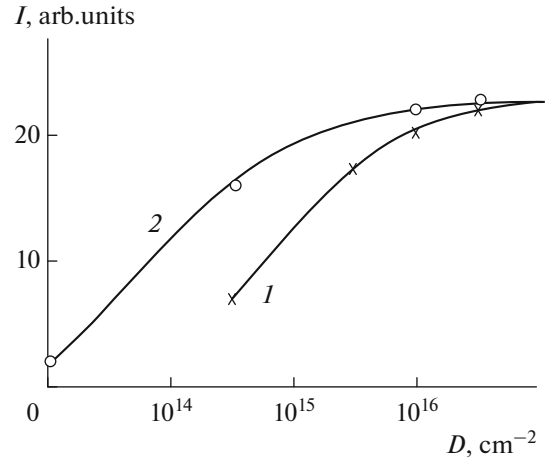

Fig. 1. Dependence of the Auger-peak intensity of oxygen on the irradiation dose of Si implanted with O_2^+ ions of the energy $E_0 = 1$ keV: (*1*) on the surface; (*2*) at a depth of ~25 Å.

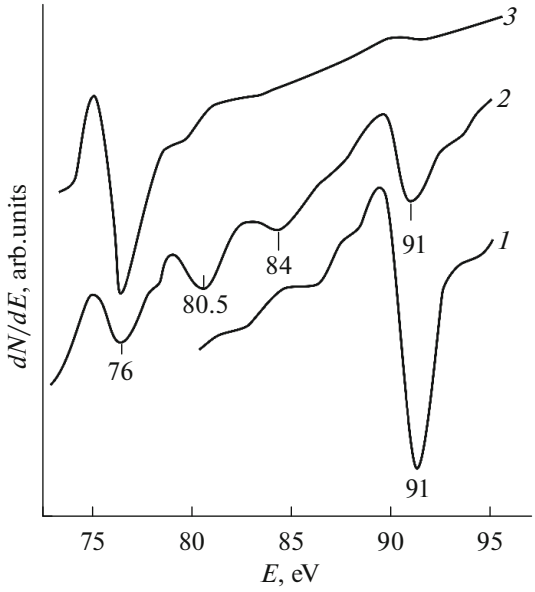

Fig. 2. Auger spectra of the Si(111) sample in the energy region of $E \approx 70$–100 eV: (*1*) initial; (*2*) implanted with O_2^+ ions of the energy $E_0 = 1$ keV at $D = 6 \times 10^{16}$ cm^{-2}; (*3*) after annealing at 900 K.

6×10^{16} cm^{-2}. After each cycle of ion implantation, the sample was annealed at the temperature of formation of a SiO_2 type compound of ~850–900 K for 40 min [11]. First, the Auger spectra of the Si surface, and then of the surface region at a depth of 25–30 Å were measured. The surface was etched by bombardment with Ar^+ ions.

RESULTS AND DISCUSSION

Figure 1 shows the dependence of the intensity I of the Auger peak of O ($E \approx 506$ eV) on the irradiation dose for Si implanted with O_2^+ ions of $E_0 \approx 1$ keV. Curve *1* refers to the variation of I on the surface, and curve *2* refers to that at a depth of ~25 Å, which corresponds to the maximum of the distribution of oxygen atoms near the surface. Figure 1 shows that the oxygen concentration in the surface layer is much higher than that on the surface. At an ion-irradiation dose of $D \geq 5 \times 10^{16}$ cm^{-2} both dependences reach a plateau, i.e., the oxygen concentration on the surface and in the surface layer up to a depth of 25–30 Å is distributed almost equally. A SiO_2 film with a thickness of ~25–30 Å is formed after annealing at $T \approx 850$–900 K. Based on this, it can be concluded that nanocluster phases and layers of silicon oxide are formed first in the surface layer at a depth where the oxygen distribution maximum is observed. As the ion dose increases, the oxide film grows towards the surface [12–15].

Figure 2 shows the initial part of the spectrum of Auger electrons of Si implanted with O_2^+ ions of $E_0 = 1$ keV at $D = 6 \times 10^{16}$ cm^{-2} measured before and after annealing at 900 K for 40 min. It can be seen that after the implantation of oxygen ions with $E_0 = 1$ keV the intensity of the Si Auger peak $L_{23}VV$ ($E_{\text{Auger}} = 92$ keV) decreases sharply, and peaks at an energy of 84 and 80.5 eV, typical for Si suboxides (SiO, $SiO_{0.5}$), and a peak at $E = 76$ eV for SiO_2 appear near it. Analysis of the complete Auger-electron spectrum showed that the Si surface contains ~30–35 at % of SiO_2, ~40–45 at % of Si suboxides, and also unbound Si (~10–15 at %) and O (5–10 at %) atoms [16].

The concentration of atoms on the surface and in the surface layer was determined from the change in the intensities of the main high-energy peaks of O (506 eV) and Si (1614 eV) according to the well-known formula:

$$C_x = \frac{I_x/S_x}{\sum I_x/S_x},$$

where I is the peak intensity of the corresponding element, and S is the Auger sensitivity coefficient of this element.

The concentration of SiO_2, Si suboxides and excess Si atoms was estimated by the change in the area under the Si peak $L_{23}VV$ at 91 eV before and after ion implantation. After ion implantation, the area under the pure Si peak decreases by about seven times (Fig. 2, curve *2*), i.e., it can be assumed that the concentration of pure Si is ~10–15 at %, and Si in a concentration of ~75–80 at % forms a chemical bond with oxygen. The ratio of the areas under the Si + O peaks was used to estimate the concentrations of SiO_2, SiO and $SiO_{0.5}$. After annealing at 900 K the Auger peaks of Si, O and Si suboxides disappear completely, and the intensity of

Table 1. Band-energy parameters of the initial sample Si(111) and that implanted with O_2^+ ions with an energy of 1 keV

Parameters	Sample		
	initial	300 K	900 K
$e\varphi$, eV	4.5	4.7	4.1
$e\Phi$, eV	5.1	5.9	8.9
E_g, eV	1.1	2.3	7.9
χ, eV	4	3.6	1.0

$e\varphi$ is the thermionic work function, $e\Phi$ is the photoelectric work function, E_g is the band gap, χ is the electron affinity (in the case under consideration, it is equal to the width of the conduction band).

the Auger peak of SiO_2 at $E = 76$ eV increases to the greatest extent (curve *3*).

Figure 3 shows the photoelectron spectra of single-crystal Si(111) implanted with O_2^+ ions of $E_0 = 1$ keV at $D = 6 \times 10^{16}$ cm^{-2} obtained at $h\nu = 21.2$ eV before and after annealing at 900 K. The Si(111) spectrum exhibits peaks due to the excitation of electrons from the surface states and the $3p$, $3s + 3p$, $3s$ states of valence electrons. After ion implantation, the shape and structure of the energy distribution curve of single-crystal Si(111) changes dramatically; the density of electron states of the valence band and the parameters of the energy bands of pure and ion-implanted Si differ significantly from each other. As shown above, these changes are related to disordering of the surface layers,

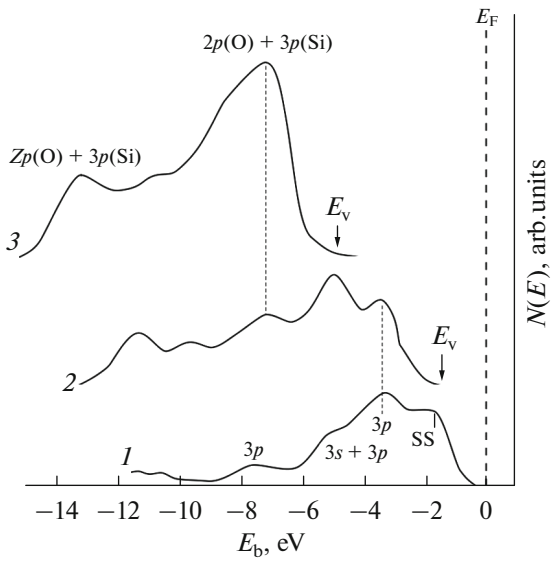

Fig. 3. Photoelectron spectra: (*1*) pure Si(111); (*2*) implanted with O_2^+ ions of the energy $E_0 = 1$ keV at $D = 6 \times 10^{16}$ cm^{-2}; (*3*) SiO_2 prepared by annealing at 900 K of ion-implanted Si. SS issurface state.

the formation of various silicon oxides, and the presence of unbound Si and O atoms [10, 16–18]. Therefore, the photoelectron spectrum of ion-implanted Si has a very complex structure, and features associated with the presence of various compounds and unbound atoms are observed in it (Fig. 3, curve *2*). The positions of some peaks approximately coincide with those of Si (3.6 eV) and SiO_2 (7.2 eV). A continuous SiO_2 film with a thickness of $d \approx 25$–30 Å is formed after annealing. Two maxima are clearly distinguished in the spectrum of the SiO_2 film. The maximum at $E_b = 7.2$ eV is apparently due to hybridization of the Si3*p* and O2*p* states, and the maximum at $E_b \approx 13.2$ eV is associated with the hybridization of Si3*s* and O2*p* states. Based on analysis of the spectra of photoelectrons and elastically reflected electrons, the energy parameters of the electron bands of ion-implanted Si before and after annealing at 900 K were determined (Table 1).

It can be seen from Table 1 that the energy parameters of the Si(111) bands change sharply after ion implantation. In particular, the E_g value is doubled, which may be due to the presence of non-stoichiometric SiO_x oxide in the ion-doped layer. Post-implantation annealing at 900 K leads to the formation of a continuous layer of SiO_2 oxide; therefore, the E_g value increases to 7.9 eV [19].

CONCLUSIONS

It has been established that $SiO_{0.5}$, SiO and SiO_2 oxides are formed in the ion-doped layer after the implantation of O_2^+ ions with $E_0 = 1$ keV at $D = 6 \times 10^{16}$ cm^{-2}. A uniform continuous SiO_2 film 25–30 Å thick was formed after annealing at 900 K. It has been shown that nanocluster SiO_2 phases are formed at ion implantation with a dose of $D \le 5 \times 10^{15}$ cm^{-2} after annealing at a depth of 25–30 Å. Starting with a dose of $D \approx 5 \times 10^{15}$ cm^{-2}, the cluster phases, the boundaries of which overlap, form the SiO_2 layers. At a further increase in the ion dose, the oxide film grows towards the surface, and at $D \ge 5 \times 10^{16}$ cm^{-2} the thickness reaches a plateau. The density of state of electrons in the valence band has been studied for the first time and the band-energy parameters of Si implanted with O_2^+ ions of a dose of ~6×10^{16} cm^{-2} were determined before and after annealing at 900 K.

CONFLICT OF INTEREST

I declare that I have no conflicts of interest.

REFERENCES

1. E. S. Demidov, A. N. Mikhaylov, A. I. Belov, M. V. Karzanova, N. E. Demidova, Yu. I. Chigirinskii, A. N. Shushunov, D. I. Tetelbaum, O. N. Gorshkov,

and E. A. Evropeitsev, Phys. Solid State **53**, 2415 (2011). https://doi.org/10.1134/S1063783411120067

2. D. G. Gromov, O. V. Pyatilova, S. V. Bulyarskii, A. N. Belov, and A. A. Raskin, Phys. Solid State **55**, 619 (2013). https://doi.org/10.1134/S106378341303013X
3. K. Hoppe, W. R. Fahrner, D. Fink, S. Dhamodoran, A. Petrov, A. Chandra, A. Saad, F. Faupel, V. S. K. Chakravadhanula, and V. Zaporotchenko, Nucl. Instrum. Methods Phys. Res., Sect. B **266**, 1642 (2008). https://www.doi.org/10.1016/j.nimb.2007.12.069
4. S. B. Donaev, A. K. Tashatov, and B. E. Umirzakov, J. Surf. Invest.: X-ray, Synchrotron Neutron Tech. **9**, 406 (2015). https://www.doi.org/10.1134/S1027451015020263
5. F. Rochet, G. Dufour, H. Roulet, B. Pelloie, J. Perriere, E. Fogarassy, A. Slaoui, and M. Froment, Phys. Rev. B **37**, 6468 (1988). https://www.doi.org/10.1103/PhysRevB.37.6468
6. B. E. Umirzakov, D. A. Tashmukhamedova, M. A. Tursunov, Y. S. Ergashov, and G. Kh. Allayarova, Tech. Phys. **64**, 1051 (2019). https://doi.org/10.1134/S1063784219070260
7. B. E. Umirzakov, R. K. Ashurov, and S. B. Donaev, Tech. Phys. **64**, 232 (2019). http://www.doi.org/10.1134/S1063784219020269
8. S. Takeoka, M. Fujii, and S. Hayashi, Phys. Rev. B **62**, 16820 (2000). https://doi.org/10.1103/PhysRevB.62.16820
9. R. Krishnan, Q. Xie, J. Kulik, X. D. Wang, S. Lu, M. Molinari, Y. Gao, T. D. Krauss, and P. M. Fauchet, J. Appl. Phys. **96**, 654 (2004). https://www.doi.org/10.1063/1.1751632
10. D. A. Tashmukhamedova, M. B. Yusupjanova, G. Kh. Allayarova, and B. E. Umirzakov, Tech. Phys. Lett. **46**, 972 (2020). https://doi.org/10.1134/S1063785020100144
11. Yu. K. Undalov and E. I. Terukov, Semiconductors **49**, 867 (2015). https://doi.org/10.1134/S1063782615070222
12. D. A. Tashmuhameva, M. B. Yusupjanova, and B. E. Umirzakov, Tech. Phys. **61**, 627 (2016).
13. V. F. Zinchenko, K. V. Lavrent'ev, V. V. Emel'yanov, and A. S. Vatuev, Tech. Phys. **61**, 187 (2016).
14. Yu. K. Undalov and E. I. Terukov, Semiconductors **49**, 867 (2015). https://doi.org/10.1134/S1063782615070222
15. D. A. Tashmukhamedova and M. B. Yusupjanova, J. Surf. Invest.: X-ray, Synchrotron Neutron Tech. **10**, 1273 (2016).
16. E. V. Parinova, Candidate's Dissertation in Mathematics and Physics (Voronezh State Univ., Voronezh, 2016).
17. B. E. Umirzakov, D. A. Tashmukhamedova, G. Kh. Allayarova, and Zh. Sh. Sodikzhanov, Tech. Phys. Lett. **45**, 356 (2019). https://doi.org/10.1134/S1063785019040175
18. Y. S. Ergashov, D. A. Tashmukhamedova, and E. Rabbimov, J. Surf. Invest.: X-ray, Synchrotron Neutron Tech. **9**, 350 (2015). https://doi.org/10.1134/S1027451015020287
19. Y. S. Ergashov, D. A. Tashmukhamedova, and B. E. Umirzakov, J. Surf. Invest.: X-ray, Synchrotron Neutron Tech. **11**, 480 (2017).

Translated by L. Mosina